Chapter 10

Electronic Structure and Chemical Reactivity of Metal Oxides–Water Interfaces

Thanh N. Truong[1], Michael A. Johnson, and Eugene V. Stefanovich

Henry Eyring Center for Theoretical Chemistry, Department of Chemistry, University of Utah, 315 South 1400 East, Room Dock, Salt Lake City, UT 84112
[1]Corresponding author: Truong@chemistry.utah.edu

We present our recent progress in studying electronic structure and chemical reactivity of metal oxide-water interface. Particularly, we examined both molecular adsorption and dissociative chemisorption of water at the MgO(100)-water interface using the CECILIA (Combined Embedded Cluster at the Interface with LIquid Approach) model. This model combines advances in dielectric continuum solvation models for describing polarization of the liquid with the embedded cluster approach for treating interactions in the solid. Comparisons with results from detailed molecular dynamics and Monte Carlo simulations and with experiments were made.

Introduction

Ion sorption and chemical reactions at interfaces between metal oxides and water are central features in many natural and industrial processes. Examples include transportation of groundwater contaminants, electrode phenomena, corrosion, and dissolution. For geochemistry and atmospheric chemistry, surfaces of metal oxides are of particular interest as these compounds are major components of rocks, soils, and airborne dust particles. For many oxides it has been found that water molecules dissociate upon contact with the surface, forming various types of surface hydroxyl groups. It is also well established that these hydroxyl groups play a decisive role in many chemical properties of oxide surfaces, including ion sorption, dissolution, and catalytic activity [1].

MgO surfaces and their interactions with water provide an excellent example for the discussion of this chapter due to its extensive theoretical and experimental literatures. However, the primary reason for choosing the MgO-water system is the previously unsettled problem regarding chemical reactivity of the most stable MgO(100) surface toward water molecules that the recent theoretical method presented in this chapter had help to resolve. In particular, many previous experimental [2-5] and theoretical [6-10] studies have found that water molecules do not dissociate upon adsorption on the MgO(100) crystal surface from vacuum. However, there are several experimental indications that water can dissociate at the MgO(100)-water interface. For example, the naturally occurring transformation of mineral periclase (MgO) to thermodynamically favored brucite ($Mg(OH)_2$) implies surface hydroxylation as an intermediate step. The commonly used argument to explain this transformation requires the involvement of low-coordinated surface sites [3, 11-14] or high Miller index surface planes [9, 15-17]. It is worthwhile to note that such defective structures are minority sites at the MgO surface. Moreover, this argument does not explain the independence of the initial rate of dissolution on the presence of defects and the formation of (100) facets upon immersion of MgO crystallites in water [18]. In addition, experimental studies show that the (100) surface dissolves in liquid water [19], and the rate of dissolution increases with increasing acidity [20]. It is also known that the presence of water can radically alter reaction mechanisms and kinetics at MgO surfaces [21]. All these facts suggest that hydroxylation of the MgO(100)-water interface is quite likely.

In this chapter, we discuss applications of our recently proposed quantum embedded cluster methodology, called CECILIA (Combined Embedded Cluster at the Interface with LIquid Approach) [22, 23] to address the electronic structure and chemical reactivity at the MgO-water interface [24, 25]. The CECILIA model combines advantages of the embedded cluster method [26-28] with the dielectric continuum method for solvation to provide an accurate description of bond-forming and -breaking processes and interactions of adsorbates and surface defects with the crystal lattice and solvent. Since the details of the CECILIA model have already been discussed in several previous reports [22, 23], we briefly discuss it below.

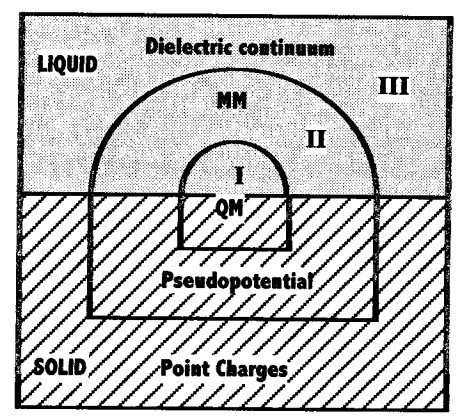

Figure 1: Schematic of the CECILIA model

A Physical Model of the Solid-Liquid Interface

In the CECILIA approach, the whole system (surface defect + crystal + solvent) is divided into three main regions (Figure 1) designed to maximize the chemical accuracy while keeping the problem tractable by modern computers.

I. The innermost QM (quantum mechanics) region, where chemistry occurs, is treated by an accurate *ab initio* molecular orbital (MO) or density functional theory (DFT). Normally, the QM cluster may consist of several lattice atoms near the defect site, the adsorbate and a couple of water molecules making strong hydrogen bonds with the surface complex. The size of this region, level of theory, basis set, and use of effective core pseudopotentials are dictated by the specific problem and available computational resources.

II. The buffer or MM region normally includes several dozen atoms in the crystal lattice surrounding the QM cluster and several solvent molecules. This region is designed to describe short-range forces between nuclei and electrons in the QM cluster and surrounding medium.

III. The peripheral zone containing point charges and a dielectric continuum ensures correct Madelung and long-range solvent polarization potentials in the quantum cluster region. This is important for an accurate representation of the cluster electron density, correct positions of the crystal electronic band edges with respect to vacuum, and redox potentials of molecular solutes. As described in several of our previous studies [23, 29, 30] several hundred point charges are often sufficient to reproduce the Madelung potential in the cluster region with an error of less than 1%. This is done by dividing the Madelung potential into two components. The component from region that is closed to the buffer zone is represented by a set of point charges located at the lattice positions. The other component is from the remaining extended crystal. This can be represented by a set of surface charges using our SCREEP (Surface Charge Representation of External Electrostatic Potential) method proposed earlier [31]. A self-consistent treatment of the solvent polarization can be achieved by using dielectric continuum solvation methods [32, 33]. We adopted the GCOSMO method documented in the literature [34-37]. It is important to point out that the COSMO boundary condition [38] does not strictly require the boundary to be a closed surface. Dispersion-repulsion contributions to the solvation free energy were calculated using Floris and Tomasi's method [39], in conjunction with OPLS force field parameters [40]. Cavitation energy was calculated using a method suggested by Pierotti [41], Huron and Claverie [42].

Computational Details

We used the cluster shown in Figure 2 to model the MgO(001) surface. For computational feasibility, ionic cores were approximated by effective core pseudopotentials (ECP) [43]. We used the standard valence CEP-31++G(d,p) basis set on the atoms of the water molecule. The CEP-31G(d) basis set was used on the

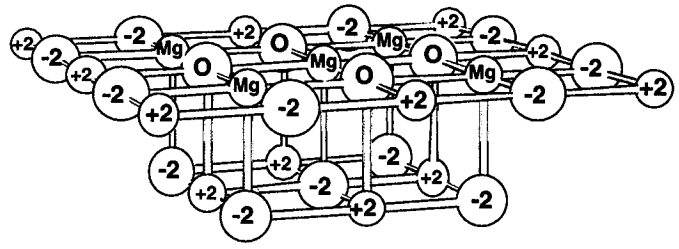

Figure 2: Cluster model of the MgO(100) surface. This cluster is embedded in the field generated by 222 additional point changes (not shown).

four oxygen ions (labeled "O") nearest to the central Mg ion. The additional diffuse functions on the water oxygen atom allow for more accurate description of adsorbate-surface interaction and were found to have only a small effect on the density of states spectra even for the dissociated chemisorption case. Oxygen ions marked as "-2" in Figure 2 were modeled as point charges (q_0 = -2) without basis functions. The CEP-31G basis set was placed on the five Mg ions at the surface (labeled "Mg"); other Mg ions in the cluster (labeled "+2") were approximated by bare pseudopotentials without basis sets. In order to represent the rest of the crystal, the cluster described above was embedded in the field generated by 222 lattice point charges of ±2 (not shown in Figure 1) so that the entire system (cluster + point charges) consisted of four stacked 8 x 8 layers resulting in an 8 x 8 x 4 slab. This finite lattice has been shown to provide an accurate Madelung potential at the (001) rock salt crystal surface without the need of using SCREEP surface charges [29, 30].

We used a Solvent-Excluding Surface [44], and the cavity boundary generated by the GEPOL93 algorithm [44] was truncated so that only adsorbed atoms and surface ions of Figure 2 were solvated. Atomic radii for cavity construction were taken from our previous work: 1.172 Å for H, 1.576 Å for O [45]. The atomic radius for Mg (1.431 Å) was fitted to the experimental hydration free energy of the Mg^{2+} ion.

Geometry optimizations, where adsorbate atoms were fully relaxed and all surface ions were held fixed at ideal lattice positions, were performed using the Hartree-Fock (HF) theory. Electron correlation corrections were estimated by performing single-point second order Møller-Plesset perturbation theory (MP2) calculations at HF optimized geometries.

In characterizing the surface electronic structure of cluster and adsorbed water configurations considered in this work, we present results for the electronic density of states (DOS). This information can be useful for qualitative analysis of data collected in electron spectroscopy experiments [13, 46-49]. As suggested earlier [47], to attain the best agreement between calculated density of states and experimental UPS and MIES spectra for MgO, our DOS graphs were generated by smoothing of orbital energy levels with Gaussian functions having a width of 1.0 eV at half-maximum.

All calculations were performed using our locally modified GAUSSIAN92/DFT computer code[50].

Results and Discussion

We focus the discussion below only on the molecular and dissociate adsorption of water at the MgO(100)-water interface. Adsorption at the MgO(100)-vacuum interface has been addressed in numerous reports and thus does not need to be included here. Of particular interest to the discussion below are the comprehensive MD and MC simulation results on the structure and dynamics of molecular water at the MgO-water interface performed by McCarthy *et al.*[8] and the experimental metastable impact electron spectroscopy (MIES) results for the detection of hydroxyl species from dissociative chemisorption of water at the water covered MgO(100) surface done by Goodman and co-workers [51]. In these simulations, 2-D periodic boundary condition with unit cells of 64 and 128 water molecules was used. This corresponds to several layers of water above the MgO surface. Interactions between water molecules were represented by the SPC potential force field whereas interactions between water and MgO surface were described by a force field fitted to results from *ab initio* periodic electronic structure calculations. In MIES, metastable excited helium atoms were utilized to eject electrons from the substrate surface. In the case of insulating surfaces, the intensity of the ejected electrons versus their kinetic energy gives a direct image of the density of occupied states of the surface. Since the metastable helium atoms approach the surface with thermal kinetic energy of about 200 meV this technique is nondestructive and highly surface sensitive, thus it is able to distinguish molecular and dissociative adsorption species of water at the water-covered MgO(100) interface.

Molecular adsorption

The average structure of H_2O adsorbed at the MgO-water interface (see Table 1) is slightly different from that at the MgO-vacuum interface. The noticeable difference is an increase in the tilt angle by 3.3 degrees. This is in reasonable agreement with calculations by McCarthy *et al.*[8] who found that in going from the MgO-vacuum to the MgO-water interface, the tilt angle changes from 105 to 107 degrees. In this study, we were not able to reproduce another configuration corresponding to the tilt angle of 60 degrees as observed in the angular distribution of near-surface water molecules [8]. This orientation probably appears as a result of cooperative interactions of several water molecules that were not included in our model. In a more recent study [52] using a 3D extended Reference Site Interaction Model (RISM) model, we were able to predict the later configuration in agreement with the MC simulations. We also found that the liquid water modeled as a dielectric continuum has very little effects on the electronic structure of the MgO surface if only molecular adsorption is assumed.

To have a better understanding on the balance of different interactions at the MgO-water interface, we plot the potential of mean force for moving the adsorbed water at the interface to the bulk liquid as a function the height of the water oxygen above the surface (O_Z). It is interesting to note that the adsorbed H_2O at the interface corresponds to a local minimum on the free energy surface but has 1.8 kcal/mol higher

Table 1: Structure (Å, degrees) and MP2 Adsorption Energy (kcal/mol) for a Water Molecule at the MgO(001) Vacuum and Aqueous Interface.

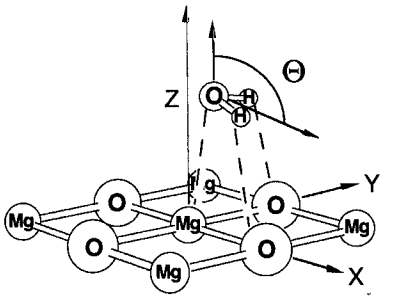

Parameter[a]	*Vacuum Interface*	*Aqueous Interface*
O-H Bond Length	0.954	0.956
H-O-H Angle	105.35	105.30
O_Z	2.32 (2.02)[b]	2.31 (2-3)[b]
$O_X = O_Y$	0.30 (0.54)[b]	0.32
Tilt Angle θ	106.7 (105)[b]	110.0 (107 or 60)[b]
Binding Energy	+14.2 (+17.3)[b]	-1.8

[a]See figure above

[b]Calculated in ref. [8].

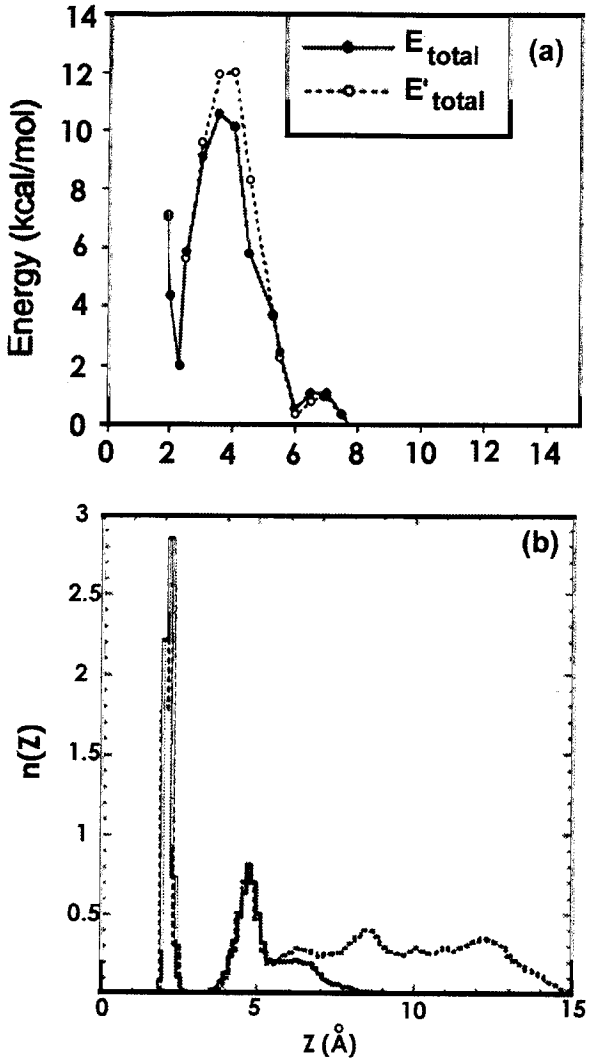

Figure 3: Characteristics of the MgO(001)-water interface as functions of distance (z) between water oxygens and the surface plane. (a) Energy profile $(E_{total}(O_z))$ *for a water molecule adsorbed at the interface calculated using the CECILIA model. (b) Density profiles previously obtained from molecular dynamics simulations (Adapted with permission from ref. [24])*

in energy than that for H_2O in bulk liquid and a barrier of about 9 kcal/mol to move the bulk as shown in Figure 3. This provides an explanation for why adsorbed water molecules rarely exchange with the bulk the MD simulations. However, the origin for such an observation appears to be much more complicated than the simple energetic argument given by McCarthy and coworkers that water molecules confined to the interface are due to the strong water-surface attraction.

We have performed a detailed analysis of the various contributions to the potential of mean force shown Figure 3 by decomposing the interfacial adsorption system in terms of three mutually interacting systems: water molecule, crystal surface, and liquid. Assuming that the total interaction energy is additive, we can write

$$E'_{total}(O_z) = E_{H_2O-surface}(O_z) + E_{H_2O-liquid}(O_z) + E_{surface-liquid}(O_z). \quad (1)$$

The three individual contributions to $E'_{total}(O_z)$ can be estimated from three separate calculations. In each of these calculations we fixed the geometry of the water molecule to be the same as in the case of $E_{total}(O_z)$. The three interaction curves, as well as the sum represented by $E'_{total}(O_z)$ above, are shown in Figure 4.

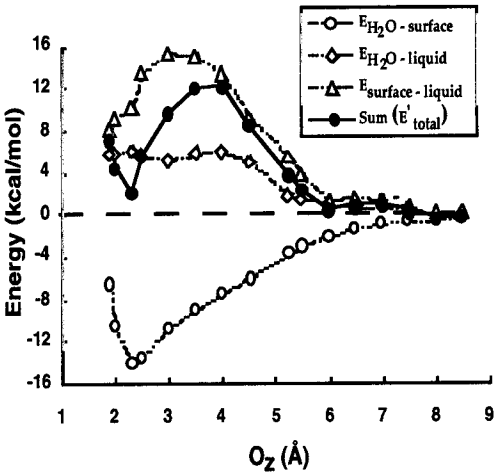

Figure 4: The total interaction energy (solid line) of a water molecule at the MgO-water interface as the sum of three distinct interactions (see eq 1). (Adapted with permission from Ref. [24])

For $E_{H_2O-surface}(O_z)$ we calculated the energy profile for molecular water desorption from the bare MgO surface represented by the embedded cluster without the dielectric continuum present. This gives a familiar interaction curve with a deep minimum of -14 kcal/mol.

For $E_{H_2O-liquid}(O_z)$, the crystal lattice was removed while the dielectric cavity surrounding the surface atoms (at a distance of 1.4-1.6 Å from the crystal surface) and the water molecule remained. This type of calculation resembles the situation that exists when a water molecule penetrates into bulk liquid through the liquid-gas interface. Energy gradually decreases as H_2O penetrates deeper into the bulk liquid and the difference is the free energy of solvation of water.

The curve for $E_{surface-liquid}(O_z)$ was obtained in calculations where the water molecule was absent but the shape of the dielectric cavity above the MgO surface was the same as if the water molecule were present. This plot represents changes in hydration energy of the MgO surface cluster as the shape of the hydration cavity varies in the process of H_2O desorption. $E_{surface-liquid}(O_z)$ has a broad maximum extending from 2 to 6 Å outward from the crystal surface. This barrier originates from a reduction in electrostatic hydration of the MgO surface and a larger cavitation energy due to the increased size of the dielectric cavity when a water molecule moves away from the surface.

As seen in Figure 4 the sum of the three energy components (shown as a broken line) indeed serves as a good approximation to the total interaction energy at the MgO-water interface. At small values of O_Z ($\leq$ 2 Å), the leading contribution comes from the repulsive part of the $E_{H_2O-surface}(O_z)$ interaction. $E_{surface-liquid}(O_z)$ is largely responsible for the energy barrier on the $E_{total}(O_z)$ curve. Existence of this barrier prevents water molecules in the first adsorbed layer from exchanging freely with bulk water. In addition, instead of the strong water-surface attraction at the interface we found that due to the combined repulsive effect of $E_{H_2O-liquid}(O_z)$ and $E_{surface-liquid}(O_z)$, water molecules are thermodynamically preferred to be in the bulk.

From the analysis above it follows that energy profiles for other lateral positions of adsorbed water (as well as the energy profile averaged over O_X and O_Y) will be qualitatively similar to that presented in Figure 3(a). This allows us to conclude that the average density of water molecules near the interface should anti-correlate with the energy plot in Figure 3(a), i.e., minima on the energy plot correspond to maximum density of particles, and maxima on the energy plot indicate regions more likely to be void of water molecules. Such behavior is clearly seen from comparison of Figure 3(a) with the plot in Figure 3(b), where we have reproduced the density profile for water molecules near the MgO surface obtained in molecular dynamics simulations. The local energy minimum at 2.3 Å corresponds to a narrow sharp density peak at oxygen-surface distances of 2-2.5 Å. The energy barrier at 3-4 Å corresponds to the gap in the density profile at O_Z = 3-4 Å. Both profiles of Figure 3 indicate a homogeneous phase of water exists beyond 7 Å of the MgO(001) surface. Although there is some quantitative discrepancy, the overall qualitative agreement between the free energy profile from CECILIA calculations and the water density profile from molecular dynamics simulations is remarkable.

A. Dissociative Adsorption

The key advantage of the CECILIA model is in its ability to study reactive processes at the solid-liquid interface. Using the same procedure as for studying molecular adsorption, heterolytic dissociation of water into charged OH- and H+ at the MgO(100)-water interface is predicted to be energetically favorable. In fact we found a global minimum corresponding to the formation of two hydroxyl groups as shown in Figure 5. Here, O_WH^- is bound to the lattice Mg^{2+} ion, and the proton makes a strong bond with the lattice oxygen ion whereby its bond with oxygen from the water molecule is virtually broken (O-H distance is 2.21 Å). However, some residual attraction between OH^- and H^+ species remains which keeps the HOH angle at about 98.9 degrees, close to the value found for the free water molecule. This minimum has the adsorption energy of 11.0 kcal/mol, that is 21.0 kcal/mol lower

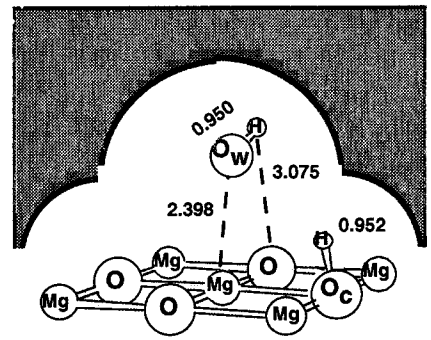

Figure 5: Optimized geometry for dissociated water at the MgO(100)-water interface ([MgO]H^+OH^-). Bond lengths are given in Å.

than for a separated adsorbed OH^--H^+ pair. Thus our calculations predict that OH^- and H^+ can exist at the MgO-water interface as nearest neighbor species, and their diffusion away from each other is not likely.

Figure 6 presents the calculated densities of states for some adsorbate configurations. To facilitate comparison with the MIES experiment, the reference zero of energy is also at the Fermi level of the molybdenum substrate. In Table 2 we list the positions of the DOS features with reference to the top of the valence band.

Theoretical positions were determined by defining the highest eigenvalue in the O(2p) band as the valence band edge. Energy differences were then taken between this reference point and the levels of interest. Shown in parentheses in Table 2 are the experimental positions of DOS features relative to the O(2p) band edge.

Table 2: Positions of DOS Features (eV) with Respect to the Top of the Valence Band. Experimental Numbers are in Parentheses.

Feature	Fig. 6b $O_cH^-(g)$	6c $O_cH^-(aq)$	6d $O_wH^-(g)$	6e $O_wH^-(aq)$	6f $O_wH^-(aq)$	6g H_2O $O_cH^-(aq)$
$1b_1$						4.3 (3.4)
$3a_1$						5.8 (5.4)
$1b_2$						9.6 (9.8)
$1\pi_W$			-2.2	2.4	1.5 (1.6)	
$3\sigma_W$			2.2	5.5	5.3 (6.1)	
$1\pi_C$	6.8	5.5			6.2	
$3\sigma_C$	10.0	8.6			9.5	

Figure 6a shows the DOS for the clean MgO(100) surface and provides a base-line for comparison to other adsorption complexes. Upon adsoprtion of H^+ (see Figure 6b), the entire spectrum shifts to higher electron binding energies relative to the MgO(100) surface. As was explained in previous studies [15, 53], this shift is due to the positive electrostatic potential generated in the cluster by the presence of a proton. The local electronic structure of the proton adsorbed on the crystal oxygen (O_C) is similar to that in an OH^- ion. This adsorption complex gives a $2\sigma_C$ peak below the oxygen 2s valence band and a double-peak structure below the O(2p) valence band [15, 54]. The latter peaks are labeled as $3\sigma_C$ and $1\pi_C$ according to the molecular orbital classification in OH^-. In the presence of water, polarization induces a negative potential in the vicinity of the H^+ adsorption site. This reduces the splitting of H^+ induced features from the crystal bands (see Figure 6c).

In agreement with other calculations [15, 54], adsorption of OH^- produces a structure in the band gap region near the top of the O(2p) valence band (labeled $1\pi_W$ in Figure 6d). The $2\sigma_W$ and $3\sigma_W$ features are hidden inside the valence bands. In the presence of water (Figure 6e), polarization induces a positive potential around OH^-, so adsorption-induced levels shift to higher binding energies and $2\sigma_W$ and $3\sigma_W$ levels appear below the oxygen 2s and 2p valence bands, respectively. In this case the $1\pi_W$ peak is inside the oxygen 2p valence band.

The DOS for water dissociated at the MgO-water interface (Figure 6f) exhibits features of both adsorbed H^+ and OH^-. All peaks, except for $1\pi_W$, are well separated from crystal bands, and the $3\sigma_W$ and $1\pi_C$ peaks overlap. In an attempt to understand how much the dielectric solvent contributes to the DOS of dissociated water, we performed a single-point calculation, at the geometry shown in Figure 5, with the solvent removed. Note that this structure does not correspond to a stable minimum at the solid-vacuum interface. The resulting DOS was virtually the same as with the solvent present (Figure 6f). This result indicates that water solvent is important for stabilizing the hydroxyl pair but does not significantly change the electronic structure of dissociated water at the MgO(100)-water interface. Recall that similar results were found for the molecular adsorption case.

The calculated DOS helped to interpret the new features on the MIES spectra upon raising the temperature on multilayer water covered MgO(100) thin film beside those ($1b_2$, $3a_1$ and $1b_1$) from the molecular adsorbed waters as shown in Figure 7. These features correspond to hydroxyl groups on the surface. We can determine from the calculated DOS the approximate nature of the hydroxyl groups that exist on this MgO surface. There are essentially three types of hydroxyls to consider: (i) a protonated surface oxygen ion; (ii) an adsorbed hydroxyl group; (iii) both (i) and (ii) in close proximity and in the presence of a solvent as in Figure 5. The calculated DOS of a type (i) hydroxyl group (Figure 6b and 6c) is distinguished by a doublet that is significantly displaced to higher binding energies from the oxygen 2p band. This is not consistent with the new features of the MIES spectra. A type (ii) hydroxyl group at the MgO-vacuum interface is characterized by a level in the band gap (Figure 6d), and the MIES spectra show no such levels. However, the positions of the hydroxyl peaks ($3\sigma_W$ and $1\pi_W$) in a type (iii) hydroxyl complex (Table 2 and

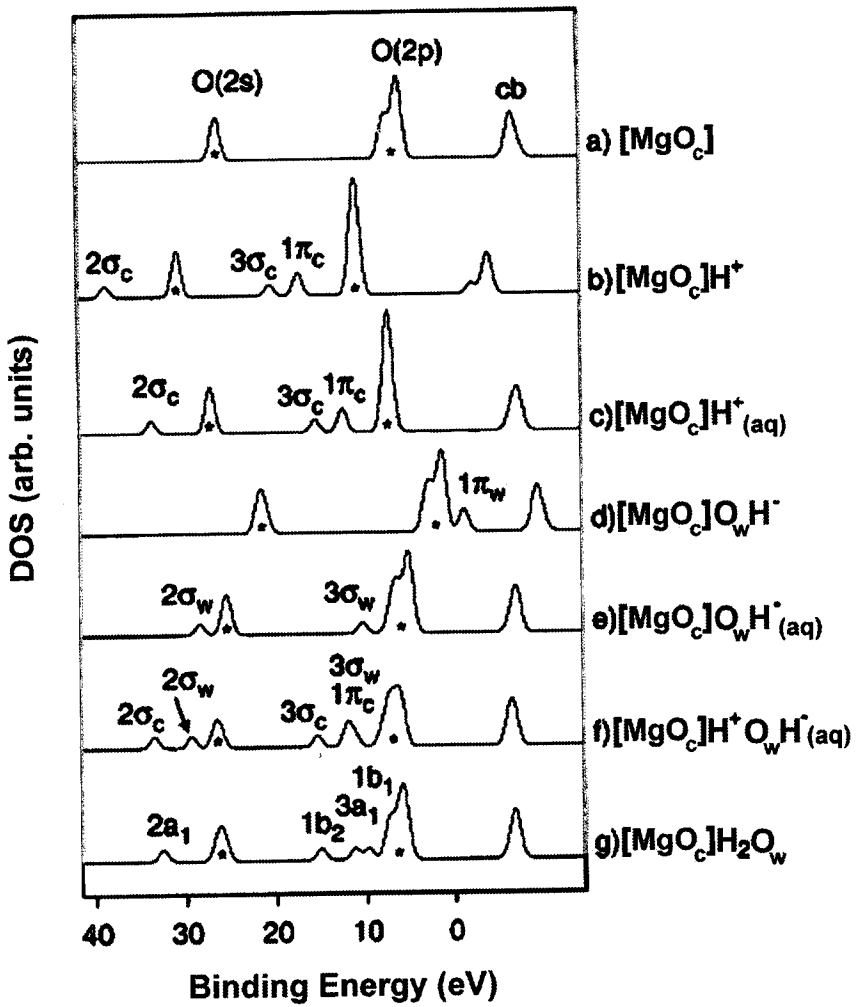

Figure 6: Calculated density of states. The conduction band states are labeled "cb", and an asterisk is used to mark the position of O(2s) and O(2p) crystal bands. "c" and "w" notations indicate features due to the O_cH^- *and* O_wH^- *hydroxyls, respectively. (Adapted with permission from Ref. [51])*

Figure 6f) are in good agreement with the MIES spectra of Figure 7. Therefore, we have assigned the two new features of the MIES spectra to the $3\sigma_W$ and $1\pi_W$ hydroxyl levels.

Molecular dynamics simulations indicate the absence of significant structure in the liquid phase beyond the first two layers of water adsorbed on MgO [8]. Therefore, water coverage of 3 ML, as in the MIES experiments, is believed to be sufficient to create a condition near the MgO crystal surface that is very similar to the MgO-water interface environment. In this multilayer coverage regime, our results indicate that water molecules dissociate at the interface; however, the hydroxyl products of such a dissociation are not seen in our spectra due to the surface sensitivity of MIES. Rather, water molecules at the top of the multilayer are visible. Upon raising the temperature, molecular water desorbs and hydroxyls become exposed at about 155 K. However, it is difficult to say how many water molecules around the OH^--H^+ pair are sufficient to keep this configuration stable. In principle, a layer of adsorbed molecular water (at 1 ML coverage) or a cluster of just a few water molecules (at submonolayer coverage) around the OH^--H^+ pair could be sufficient to stabilize this configuration. In this case, features from both adsorbed O_WH^- and molecular H_2O would be visible in MIES spectra. However, we would expect the H_2O induced peaks to be weaker than O_WH^- peaks because O_WH^- species are protruding above the layer of adsorbed water molecules laying essentially flat on the surface [8, 24, 55].

The result that hydroxylation of the MgO(100)-water interface lowers its energy offers a natural explanation for periclase transformation to brucite and dissolution of MgO in water. Low-coordinated surface sites and high-index surface planes need not be involved. Water dissociates not because the aqueous solvent increases the reactivity of the MgO surface. Based on known correlations between reactivity and ionicity of the MgO surface [30], we would expect a hydrated surface to be less reactive than the clean surface due to the slightly increased ionicity of the former. In reality, polarization of the surrounding solvent is responsible for stabilization of charged dissociation products. This result is similar to that found in the case of the NaCl-water interface [22], where solvent effects were found to be more significant in regard to interfacial reactivity than interaction with the ionic crystal surface. It is difficult to judge from our cluster calculations whether a fully hydroxylated MgO(100)-water interface is energetically stable. Answering such a question requires studies on coverage dependence of the interactions in the hydroxyl layer. This is beyond the capabilities of the CECILIA model. Another interesting question is how surface relaxation would affect the hydroxylation process. It is possible to model surface relaxation consistently within the embedded cluster model particularly for ionic crystals. We will discuss this aspect in a future study.

Conclusion

The complexity of chemical processes occurring at the solid-liquid interfaces provides a great challenge to theoretical and computational chemistry. By combining the advantages of the embedded cluster method in studying reactive processes at solid-

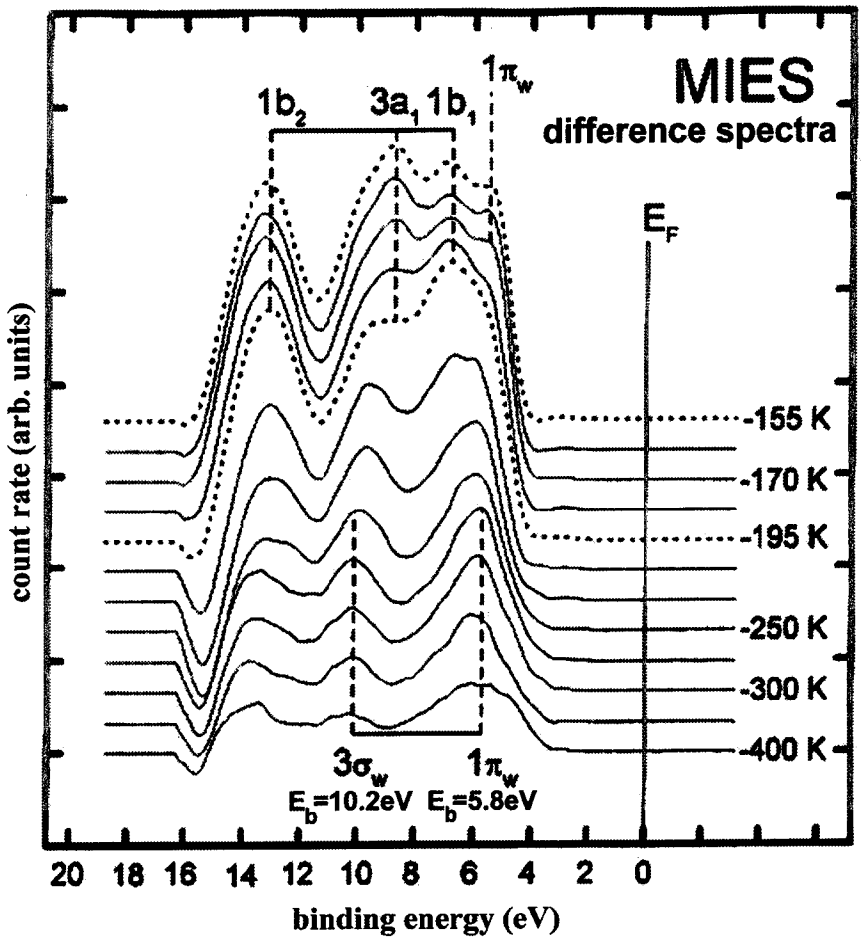

Figure 7: Differential MIES spectra (subtracting the background MgO(100) signal) taken from the MgO(100) surface covered by approximately 3 ML water, as a function of the anneal temperature. (Adapted with permission from ref. [51])

gas interfaces with the dielectric continuum solvation model for modeling reactions in solution, we were able to assemble a unified model called CECILIA. The key advantage of this model is in its ability to model chemical reactions occurring at the solid-liquid interfaces as well as the electronic structure of the interface. We have illustrated it by studying both molecular adsorption and dissociative chemisorption of water at the MgO(100)-water interfaces in comparison with recent MD and MC simulations as well as MIES experiments. We have predicted that water is dissociated at the MgO(100)-water interface in agreement with the MIES observations. More work is certainly needed in further improving the accuracy of the model, however, progress so far on the CECILIA model is very encouraging. It should be noted that the use of a dielectric continuum solvation model does not provide the liquid structure above the crystal. Recent progress in our lab of using a 3D Reference Interacting Site Model (RISM) showed great promise in providing liquid structure information at a much less computation cost comparing to MD or MC simulations [52].

Acknowledgment

This work is supported by the National Science Foundation.

References

[1] H.-P. Boehm and H. Knozinger, in *Catalysis Science and Technology*, J. R. Anderson and M. Boudart, Editors (Springer-Verlag,1983) p. 39.

[2] D. Ferry, A. Glebov, V. Senz, J. Suzanne, J. P. Toennies and H. Weiss, J. Chem. Phys., 105, (1996), 1697.

[3] M. J. Stirniman, C. Huang, R. S. Smith, S. A. Joyce and B. D. Kay, J. Chem. Phys., 105, (1996), 1295.

[4] C. Xu and D. W. Goodman, Chem. Phys. Lett., 265, (1997), 341.

[5] J. Heidberg, B. Redlich and D. Wetter, Ber. Bunsen-Gessel. Physik., 99, (1995), 1333.

[6] C. A. Scamehorn, A. C. Hess and M. I. McCarthy, J. Chem. Phys., 99, (1993), 2786.

[7] M. R. Chacon-Taylor and M. I. McCarthy, J. Phys. Chem., 100, (1996), 7610.

[8] M. I. McCarthy, G. K. Schenter, C. A. Scamehorn and J. B. Nicholas, J. Phys. Chem., 100, (1996), 16989.

[9] N. H. de Leeuw, G. W. Watson and S. C. Parker, J. Phys. Chem., 99, (1995), 17219.

[10] V. A. Tikhomirov, G. Geudtner and K. Jug, J. Phys. Chem. B, 101, (1997), 10398.

[11] Y. Kuroda, E. Yasugi, H. Aoi, K. Miura and T. Morimoto, J. Chem. Soc., Faraday Trans. 1, 84, (1988), 2421.

[12] S. Coluccia, L. Marchese, S. Lavagnino and M. Anpo, Spectrochim. Acta A, 43, (1987), 1573.
[13] H. Onishi, C. Egawa, T. Aruga and Y. Iwasawa, Surf. Sci., 191, (1987), 479.
[14] A. L. Almeida, J. B. L. Martins, C. A. Taft, E. Longo and W. A. Lester, Jr., J. Chem. Phys., 109, (1998), 3671.
[15] J. Goniakowski and C. Noguera, Surf. Sci., 330, (1995), 337.
[16] C. A. Scamehorn, N. M. Harrison and M. I. McCarthy, J. Chem. Phys., 101, (1994), 1547.
[17] K. Refson, R. A. Wogelius, D. G. Fraser, M. C. Payne, M. H. Lee and V. Milman, Phys. Rev. B, 52, (1995), 10823.
[18] R. L. Segall, R. S. C. Smart and P. S. Turner, in *Surface and Near-Surface Chemistry of Oxide Materials*, J. Nowotny and L.-C. Dufour, Editors (Elsevier,Amsterdam, 1988) .
[19] M. Komiyama and M. Gu, Appl. Surf. Sci., 120, (1997), 125.
[20] M. A. Blesa, P. J. Morando and A. E. Regazzoni, Chemical Dissolution of Metal Oxides. (CRC Press,Boca Raton, 1994).
[21] X.-L. Zhou and J. P. Cowin, J. Phys. Chem., 100, (1996), 1055.
[22] E. V. Stefanovich and T. N. Truong, J. Chem. Phys., 106, (1997), 7700.
[23] E. V. Stefanovich and T. N. Truong, in *Combined quantum mechanical and molecular mechanical methods*, J. Gao and M. A. Thompson, Editors (ACS Books,Washington, DC, 1998) p. 92.
[24] M. A. Johnson, E. V. Stefanovich and T. N. Truong, J. Phys. Chem. B, 102, (1998), 6391.
[25] M. A. Johnson, E. V. Stefanovich and T. N. Truong, J. Phys. Chem. B, 103, (1999), 3391.
[26] T. A. Kaplan and S. D. Mahanti, eds. *Electronic properties of solids using cluster methods*. Fundamental materials research, ed. M. F. Thorpe (Plenum, New York, 1995).
[27] G. Pacchioni, P. S. Bagus and F. Parmigiani, eds. *Cluster Models for Surface and Bulk Phenomena.* (Plenum, New York, 1992).
[28] R. W. Grimes, C. R. A. Catlow and A. L. Shluger, eds. *Quantum mechanical cluster calculations in solid state studies.* (World Scientific, Singapore, 1992).
[29] M. A. Johnson, E. V. Stefanovich and T. N. Truong, J. Phys. Chem. B, 101, (1997), 3196.
[30] E. V. Stefanovich and T. N. Truong, J. Chem. Phys., 102, (1995), 5071.
[31] E. V. Stefanovich and T. N. Truong, J. Phys. Chem.B, 102, (1998), 3018.
[32] J. Tomasi and M. Persico, Chem. Rev., 94, (1994), 2027.
[33] C. J. Cramer and D. G. Truhlar, in *Reviews in Computational Chemistry*, K. B. Lipkowitz and D. B. Boyd, Editors (VCH Publishers,New York, 1994) p.1.
[34] T. N. Truong and E. V. Stefanovich, Chem. Phys. Lett., 240, (1995), 253.
[35] T. N. Truong and E. V. Stefanovich, J. Chem. Phys., 109, (1995), 3709.
[36] T. N. Truong, U. N. Nguyen and E. V. Stefanovich, Int. J. Quant. Chem.: Quant. Chem. Symp., 30, (1996), 403.
[37] T. N. Truong, Int. Rev. Phys. Chem., 17, (1998), 525.
[38] A. Klamt and G. Schüürmann, J. Chem. Soc., Perkin Trans. II, (1993), 799.
[39] F. M. Floris, J. Tomasi and J. L. Pascual-Ahuir, J. Comp. Chem., 12, (1991), 784.
[40] W. L. Jorgensen and J. Tirado-Rives, J. Am. Chem. Soc., 110, (1988), 1657.
[41] R. A. Pierotti, Chem. Rev., 76, (1976), 717.

[42] M. J. Huron and P. Claverie, J. Phys. Chem., 76, (1972), 2123.
[43] W. Stevens, H. Basch and J. Krauss, J. Chem. Phys., 81, (1984), 6026.
[44] J. L. Pascual-Ahuir, E. Silla and I. Tuñon, J. Comp. Chem., 15, (1994), 1127.
[45] E. V. Stefanovich and T. N. Truong, Chem. Phys. Lett., 244, (1995), 65.
[46] J. Günster, G. Liu, V. Kempter and D. W. Goodman, J. Vac. Sci. Technol. A, 16, (1998), 996.
[47] D. Ochs, W. Maus-Friedrichs, M. Brause, J. Günster, V. Kempter, V. Puchin, A. Shluger and L. Kantorovich, Surf. Sci., 365, (1996), 557.
[48] X. D. Peng and M. A. Barteau, Surf. Sci., 233, (1990), 283.
[49] X. D. Peng and M. A. Barteau, Langmuir, 7, (1991), 1426.
[50] M. J. Frisch, G. W. Trucks, H. B. Schlegel, P. M. W. Gill, B. G. Johnson, M. W. Wong, J. B. Foresman, M. A. Robb, M. Head-Gordon, E. S. Replogle, R. Gomperts, J. L. Andres, K. Raghavachari, J. S. Binkley, C. Gonzalez, R. L. Martin, D. J. Fox, D. J. Defrees, J. Baker, J. J. P. Stewart and J. A. Pople, (Gaussian, Inc., Pittsburgh, PA, 1993.
[51] M. A. Johnson, E. V. Stefanovich, T. N. Truong, J. Günster and D. W. Goodman, J. Phys. Chem. B, 103, (1999), 3391.
[52] V. Shapovalov, T. N. Truong, A. Kovalenko and F. Hirata, Chem. Phys. Lett., 320 (2000), 186.
[53] S. Russo and C. Noguera, Surf. Sci., 262, (1992), 245.
[54] J. Goniakowski, S. Bouette-Russo and C. Noguera, Surf. Sci., 284, (1993), 315.
[55] A. Marmier, P. N. M. Hoang, S. Picaud, C. Girardet and R. M. Lynden-Bell, J. Chem. Phys., 109, (1998), 3245.